# Determination of the toroidal current density- and iota-profile in the W7-AS using soft X-ray measurements

S. Klose[1], M. Zarnstorff[2], A. Weller[3] and the W7-AS Team

[1]*MPI für Plasmaphysik, Boltzmannstr. 2, D-85748 Garching, Germany*
[2]*Princeton Plasma Physics Lab., P.O. Box 451, Princeton, NJ 08543-0451, USA*
[3]*MPI für Plasmaphysik, Wendelsteinstr. 1, D-17491 Greifswald, Germany*

## 1 Introduction

With a system of 8 pinhole cameras and 256 different lines of sight altogether, observations of the soft X-ray radiation near the triangular plane of the W7-AS were made. By using a maximum entropy tomography algorithm, the X-ray emissivity distribution ("plasma-shape") in that plane can be reconstructed, independent from the knowledge of the shape of the magnetic flux surfaces [1, 2, 3, 4].

Using the equilibrium code VMEC [5], the equilibrium magnetic flux surfaces can be calculated. Assuming that the emissivity is constant on the equilibrium magnetic flux surfaces, the theoretical expected equilibrium "plasma-shape" can be calculated.

Comparisions between the observed (tomographically reconstructed) and the theoretical expected (VMEC) equilibrium "plasma-shape" have revealed some discrepancies, in particular radial indentations [6]. These discrepancies occur primarily in net-current free (ohmic compensated) discharges with high neutral beam heating power (e.g. in "high-$\beta$" and "high-$T_i$" regimes). It will be shown, that some of these discrepancies can be explained taking a reasonable toroidal current density profile $j(r)$ into account.

To determine $j(r)$ from the soft X-ray measurements for a given total pressure profile, $j(r)$ is varied until the calculated line integrals of the VMEC equilibrium emissivity distribution best fit the measured X-ray data. The resulting $j(r)$ depends on both, the total pressure profile and the soft X-ray measurements. Therefore, it is crucial at this point to have a proper total pressure profile, determined by good enough measurements of $T_e$, $n_e$ and $T_i$ from Thomson-scattering, Li-beam, ECE and NPA diagnostic.

In the case of "high-$T_i$" discharges (e.g. #54285), the so determined $j(r)$ agrees at best to previous a priori calculations [7], because the temperature and density profiles could be measured at best in that regime, and therefore, the total pressure profile could be determined at best. Furthermore, due to the relatively high parallel electrical conductivity in that regime (compared to "high-$\beta$"), the central ohmic counter-current density is high enough to make a significant effect on the shape of the magnetic flux surfaces, even at full magnetic field (2.5 T). Therefore, the "high-$T_i$" shot #54285 will be discussed exemplarily in detail in the following paper.

## 2 Time traces of basic parameters

The "high-$T_i$" shot #54285 (Fig. 1) has a left helical magnetic field with 2.5 T, 2 MW co-NBI and 1 MW ECR heating power, and a zero total plasma current all the time (ohmic compensated). In the flat-top phase, from 200 . . . 450 ms, all parameters are nearly constant, except the soft X-radiation due to slight impurity accumulation. Hence, a small increase of the loop-voltage $U_L$ is observed, and can be interpreted as a slight decrease of the parallel conductivity $\sigma_{\|}$ due to an increase of $Z_{eff}$ during the time.

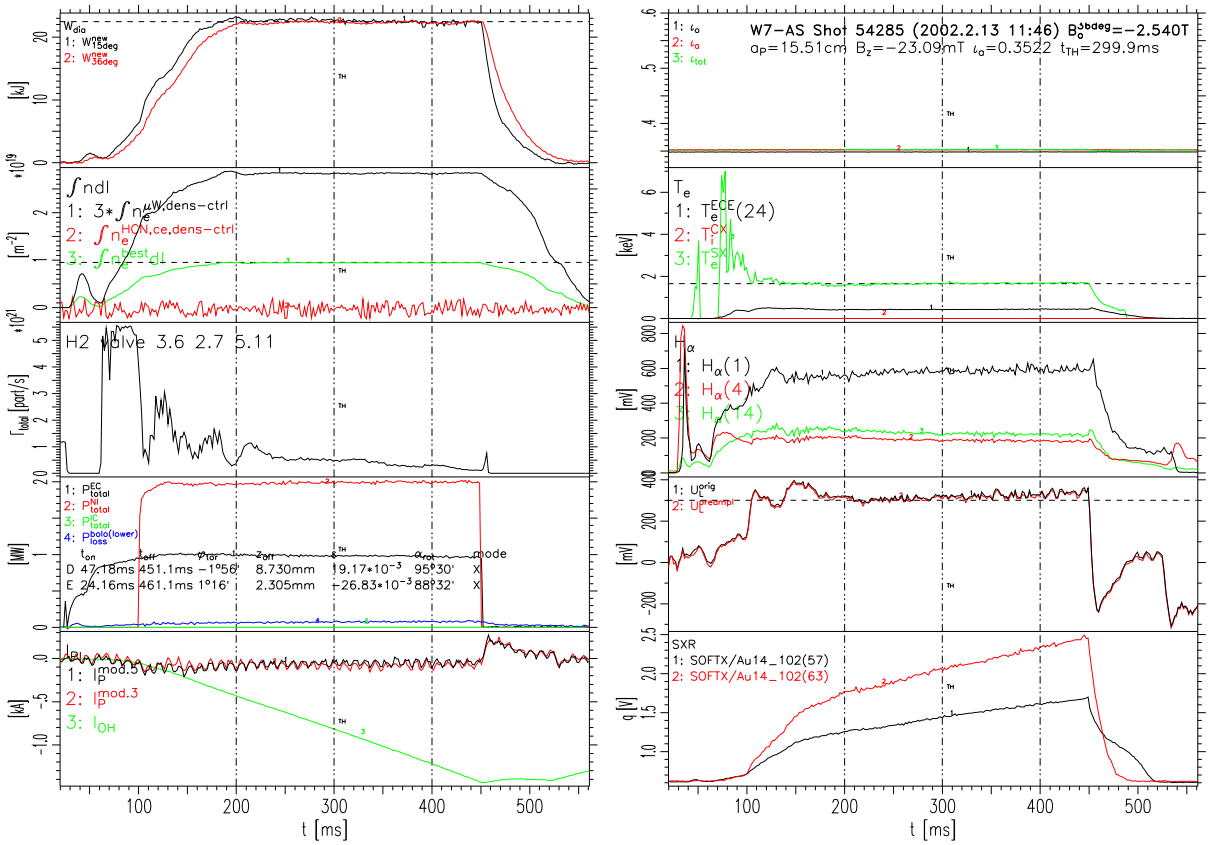


*Fig. 1: Time traces of: $W_{dia}$, $\int n_e\,dl$, $H_2$ gas flux, $P_{heat}$, $I_{pl,oh}$, iota, $T_e$, $H_\alpha$-radiation, $U_L$ and soft X-radiation.*

At $t = 300$ ms the THOMSON-scattering diagnostic measures the electron density and temperature profile. Therefore, this is the interesting time-point for the equilibrium analysis in the sections below.

## 3 Tomographic reconstruction of the soft X-ray emissivity distribution without any prior equilibrium information

At this time-point, the soft X-ray emissivity is reconstructed (Fig. 2), without[1] any prior equilibrium information (e.g. shape of the magnetic flux surfaces). The left part of this figure shows the reconstructed emissivity distribution as contour- and 3d-plot, the right part shows the measured (black crosses) and the fitted (red stars) diode signals. The fitted signals are the integrals over the reconstructed emissivity distribution, along the lines of sight.

It can be shown, that each camera profile of the diode signals is asymmetric. Hence, the reconstructed image is not circular and therefore poloidal asymmetric. To test the fit algorithm, reconstructions of similar test distributions were made. They reveal no significant artefacts in the steep gradient region of the emissivity (edge region), but slight artefacts in the central region of the distribution with much smaller gradients of the emissivity.

[1]Nevertheless, equilibrium prior-information can be used to place the quadratic reconstruction-grid optimal, in such a way, to reduce the number of grid-points with zero contribution to the diode signals (outside emitting plasma region). This reduces the number of unknown parameters and improves the resolution and accuracy of the reconstructed emissivity distribution in the region of interest.

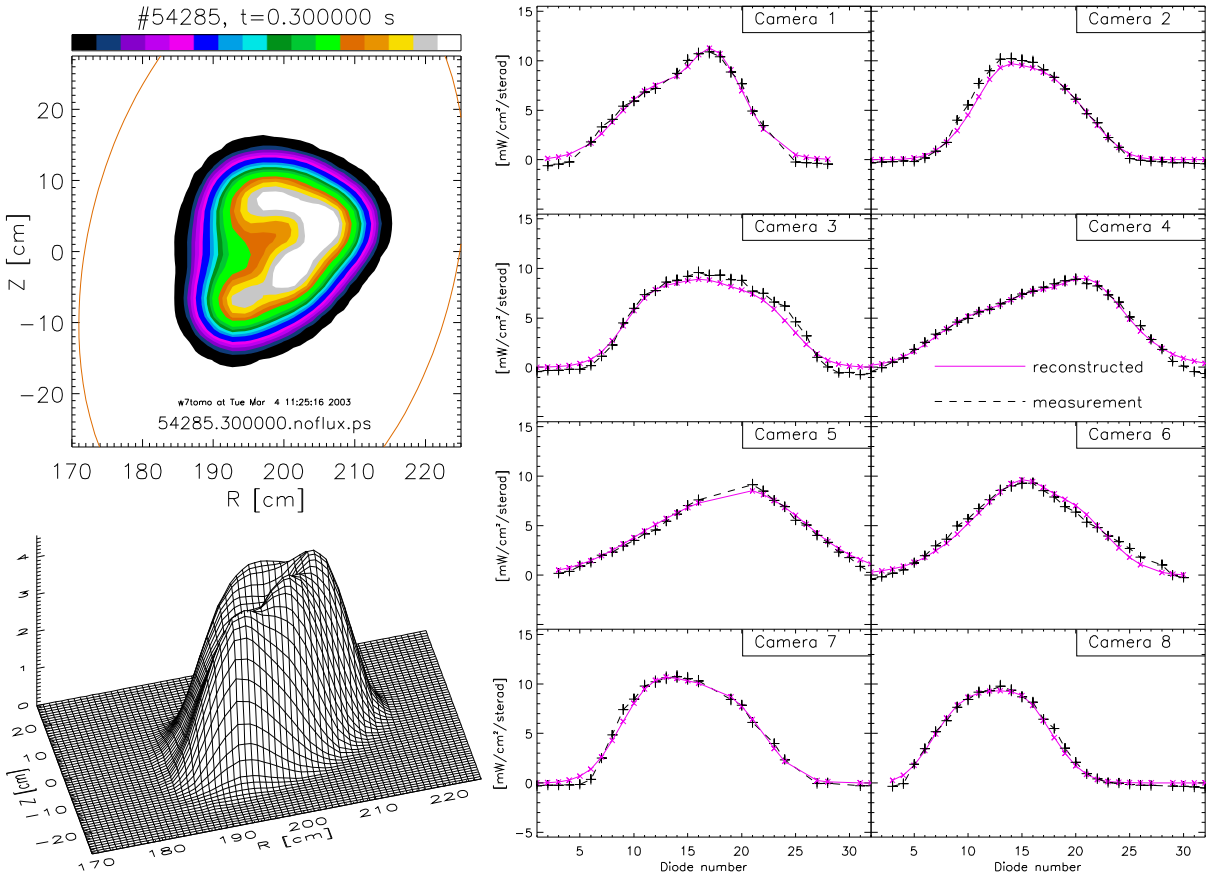


*Fig. 2: Tomographic reconstruction, independent from any equilibrium information.*

The used SXR-camera system consists of 256 rays (8 cameras with 32 diodes each), but some of the diodes (about 28) are excluded in the calculations (missing black crosses in Fig. 2), because of too bad signals. The tomographic reconstructions are made with the maximum entropy method on a quadratic grid with $20 \times 20$ pixels and $2\,\mathrm{cm} \times 2\,\mathrm{cm}$ pixel size. A measurement error of about 3 % must be taken into account for each diode. Therefore, it makes no sense to fit the emissivity distribution closer than $\sigma_{rel} \approx 0.03$ (see Eq. 3) on the data.

## 4 Obtaining the "right" pressure profile

Fig. 3 shows the measured radial profiles of $n_e$, $T_e$ and $T_i$ (thanks to A. Dinklage et. al), averaged over the flat-top phase and a continuous series of 11 identical "high-$T_i$" shots (#54285 . . . #54296, #54295 was failed). These are the best measured and most carfully evaluated profiles of all W7-AS shots, because the measurement errors of the spectroscopic diagnostics are much lower at higher $T_e$ and $T_i$, and because of some enhancements of the diagnostics and data evaluation techniques, which were done recently [8]. The primary profiles of the different diagnostics (Thomson-scattering, ECE, Li-beam, NPA) are transformed to radial magnetic flux coordinates $r_{eff}$, using a reconstructed plasma equilibrium calculated with NEMEC [9].

Fig. 4 at the top shows the total pressure- and $\beta$-profile ($n_i = n_e$)

$$p = k_B n_e (T_e + T_i) \quad \text{and} \quad \beta = \frac{p}{B^2/(2\mu_0)}\,, \tag{1}$$

calculated from the measured $n_e$, $T_e$ and $T_i$ profiles. Neglecting fast ions, the kinetic

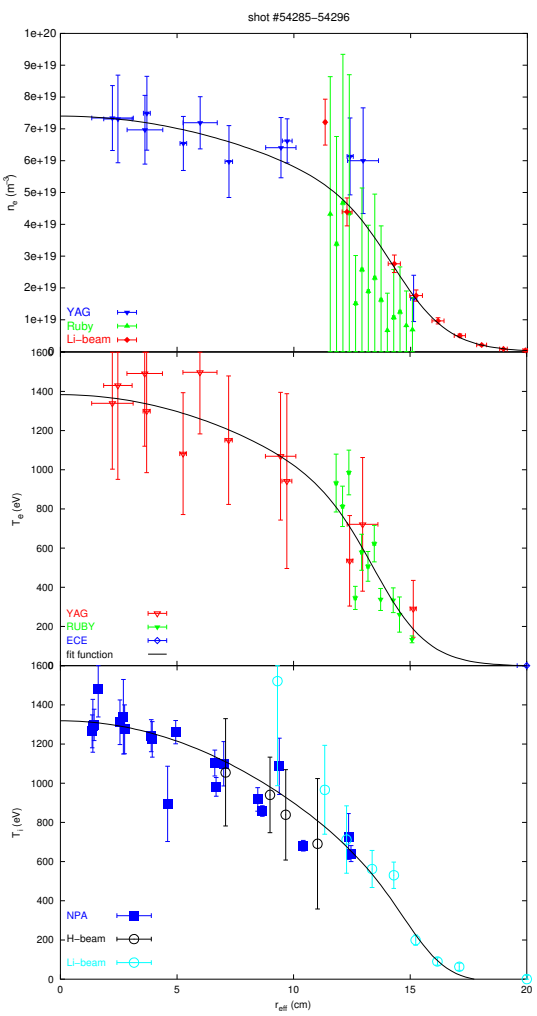


*Fig. 3: Radial profiles of $n_e$, $T_e$ and $T_i$.*

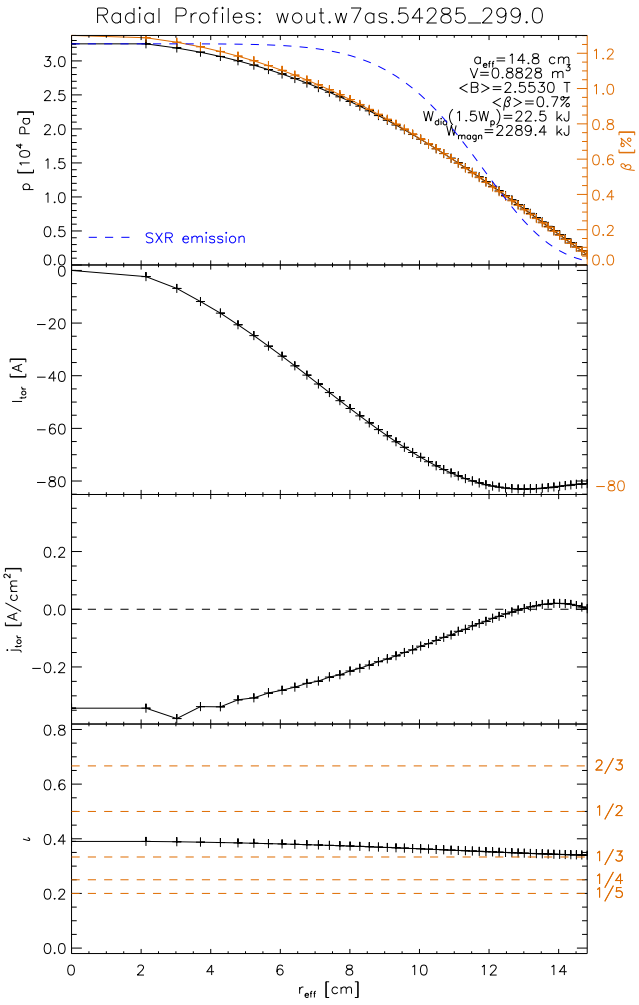


*Fig. 4: Pressure and current profiles ($j \approx 0$).*

energy

$$W_{kin} = \frac{3}{2}\, 2\pi R \left( 2\pi \int_{r=0}^{a_{eff}} p(r)\, r\, dr \right) = 22.5\,\mathrm{kJ} \approx W_{dia} \qquad (2)$$

($a_{eff} \approx 15\,\mathrm{cm}$ - minor plasma radius, $R \approx 2\,\mathrm{m}$ - major plasma radius of W7-AS) of the total pressure profile fits exactly the measured value of $W_{dia}$ (compare with Fig. 1 at $t = 300\,\mathrm{ms}$), because of, $W_{dia}$ was already used as a constraint in the fit of the profiles. This total pressure profile is used as fixed input[2] for all VMEC equilibrium calculations in this paper.

## 5 VMEC equilibrium calculation with nearly vanishing $j(r)$

At $t = 300\,\mathrm{ms}$ the total toroidal plasma current is nearly zero $I_{pl} = -80\,\mathrm{A} \approx 0$. The most trivial solution of this case is $j(r) = 0$ at all radii. Therefore, Fig. 4 shows the result of a VMEC equilibrium calculation for a nearly vanishing[3] toroidal current density $j(r)$. The

[2]The VMEC input file needs the coefficients of a power series, depending on the normalized magnetic flux coordinate, as input values for the pressure profile. These coefficients are determined with a fit of the power series on the pressure profile, using the first 4 terms.

[3]The VMEC code needs a non-vanishing $j(r)$ to avoid singularities in the calculations.

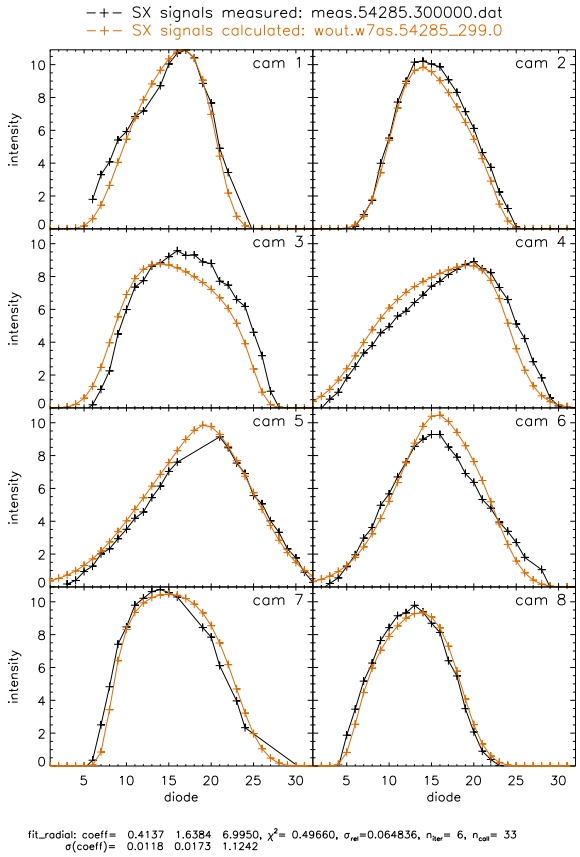


*Fig. 5: Measured and fitted signals ($j \approx 0$).*

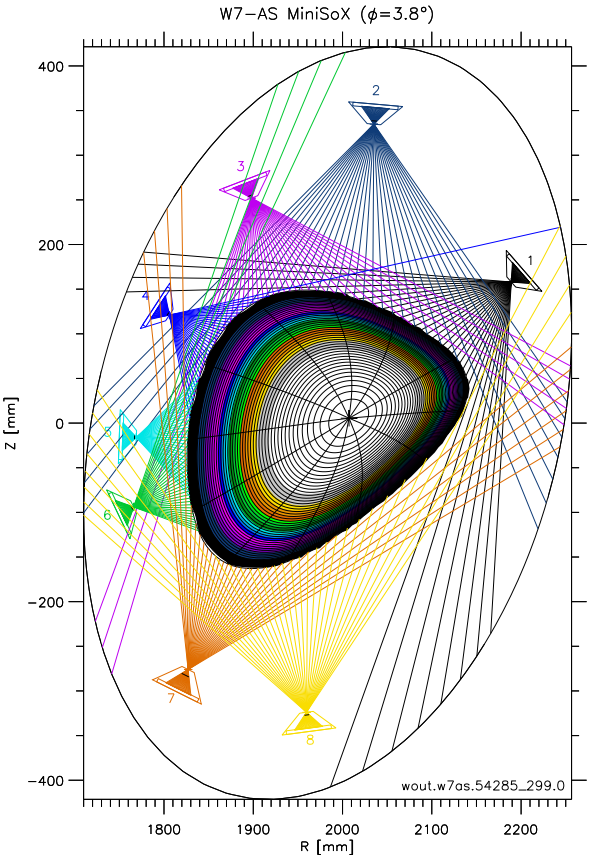


*Fig. 6: SXR emissivity distribution ($j \approx 0$).*

$\iota$-profile has negative shear and is always above 1/3.

With the assumption, that the emissivity is constant on the equilibrium magnetic flux surfaces (Fig. 6), the radial emissivity function is fitted (Fig. 4 blue dashed curve). A comparision of the measured and the calculated diode signals (Fig. 5), shows significant discrepancies between the equilibrium results and the SXR measurements. Additionally, a comparision of the resulting equlibrium emissivity distribution (Fig. 6) with the tomographic reconstruction (Fig. 2), reveals, that the emissivity of the tomogram has an indentation on the inboard plasma edge. The idea is [6], that this indentation comes from a significant non-vanishing internal toroidal current density, but still with a total toroidal current of zero.

## 6 VMEC equilibrium calculation with best fitted non-vanishing $j(r)$

Calculating the equilibrium by VMEC with different non-vanishing $j(r)$, a best fitted equilibrium can be found[4]. Fig. 7 shows the comparision of the measured and the fitted diode signals. The relative standard deviation

$$\sigma_{rel} = \frac{\chi}{\mathrm{Max}(s_i^{fit})} \quad \text{with} \quad \chi^2 = \frac{1}{n_{sig} - n_{par}} \sum_{i=1}^{n_{sig}} (s_i^{fit} - s_i^{meas})^2 \tag{3}$$

[4]This equilibrium is the best which was found so far, but, a much better fitted exist probably. The fit algorithm is not fully satisfactory at the moment, and will be improved.

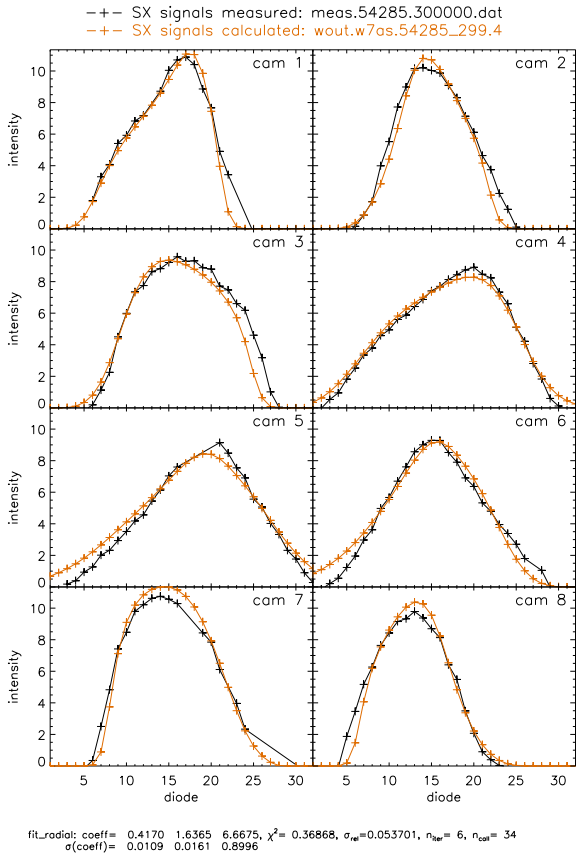


*Fig. 7: Measured and fitted signals ($j \neq 0$).*

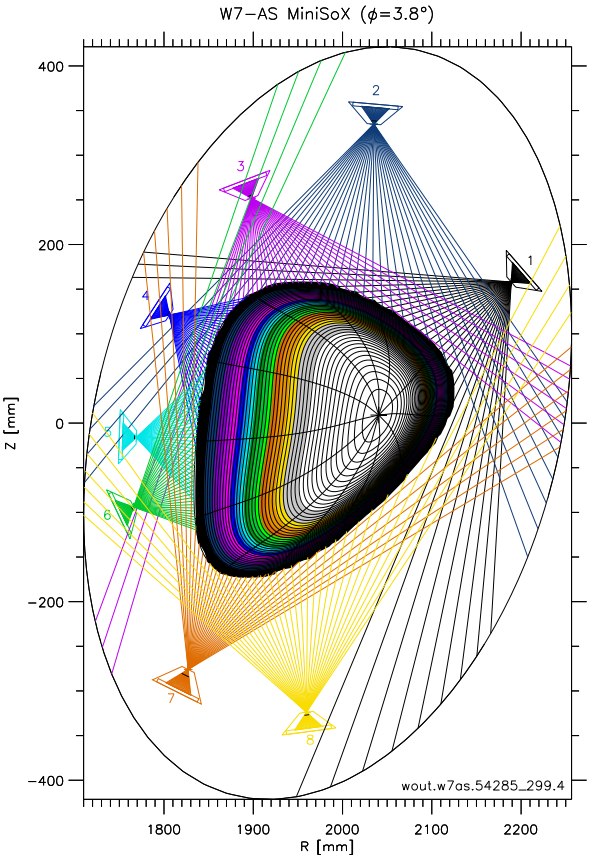


*Fig. 8: SXR emissivity distribution ($j \neq 0$).*

($s_i^{meas}$ and $s_i^{fit}$ are the measured and fitted signal values, $n_{sig} \leq 256$ and $n_{par} = 3$ are the number of signals and fit parameters), is about 1% smaller as in the nearly currentless case (Fig. 5). This is a quite small change in the fit criterion, but nevertheless, the changes in the shapes of the signal-profiles are significant.

Fig. 8 shows the corresponding emissivity distribution with the equilibrium magnetic flux surfaces. Compared to the nearly currentless case (Fig. 6), the magnetic axis is about 3 cm shifted outward, and the magnetic flux surfaces show a slight indentation on the inboard plasma edge. The "plasma-shape" is more triangular. Furthermore, the effect of the outward-shift can be seen directly in the positions of the profiles of the nearly vertical viewing cameras (2, 3 and 8). In the non-vanishing current case (Fig. 7), the maxima of the measured and calculated signal-profiles, are much better aligned, as in the nearly currentless case (Fig. 5).

The corresponding radial equilibrium profiles are shown in Fig. 9. The resulting total counter current density at the plasma axis is about $100\,\mathrm{A/cm^2}$. At the plasma edge, a co current density must exist, to balance the total current to nearly zero. The $\iota$-profile has now positive shear and is always below 1/3. At the plasma axis, $\iota$ is very small.

To estimate the amount of beam-driven and bootstrap current densities

$$j_{NBI} + j_{boot} = j - j_{OH} \ , \tag{4}$$

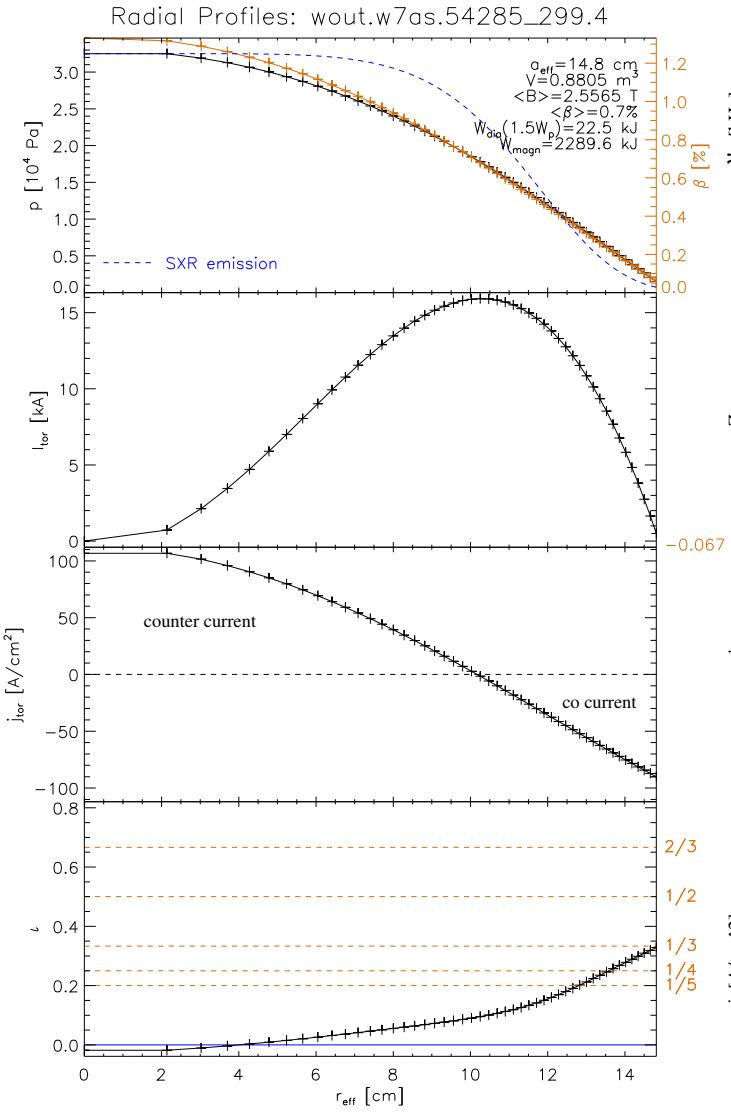


*Fig. 9: Pressure and current profiles ($j \neq 0$).*

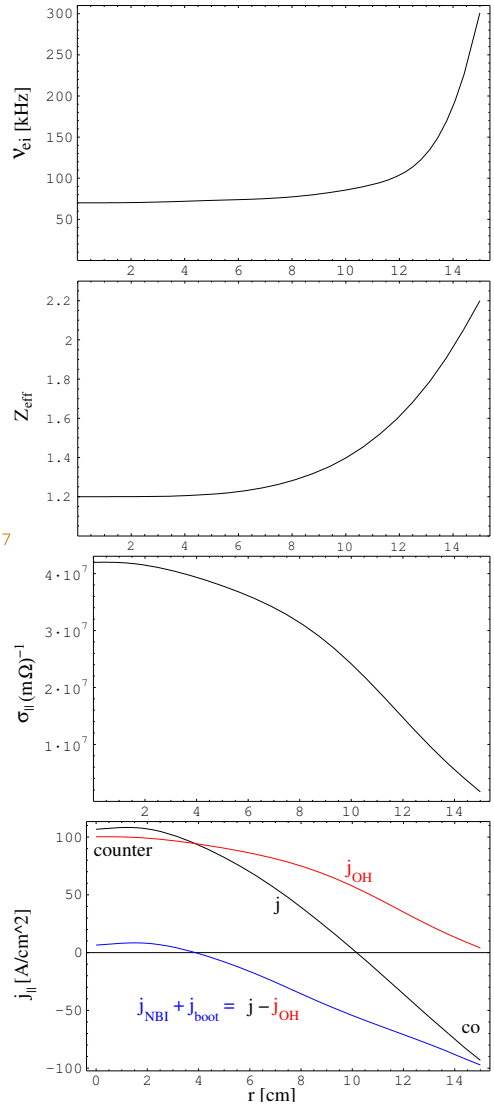


*Fig. 10: Substraction of $j_{OH}$.*

the ohmic counter current density

$$j_{OH} = \sigma_{\parallel} E_{\parallel} = \alpha(Z_{eff}) \frac{e^2 n_e}{m_e \nu_{ei}} \cdot \frac{U_L}{2\pi R} \tag{5}$$

(with the SPITZER-factor $\alpha(Z_{eff}) = 1.6\,(2 - Z_{eff}^{-1/3})/Z_{eff} \approx 0.9 \ldots 1.4$, the loop-voltage $U_L = 300\,\mathrm{mV}$ and the electron-ion collisional frequency $\nu_{ei}$) can be calculated and subtracted from the total toroidal current density (Fig. 10). The result reveals, that the NBI drives an off-axis co-current, and nearly no current inside $r \approx 4\,\mathrm{cm}$.

## 7 Comparision of the calculated equilibria with the tomographic reconstruction

To compare the calculated equilibria (Fig. 6 and Fig. 8) with the tomographic reconstruction (Fig. 2), the corresponding equilibrium flux surfaces can be plotted over (Fig. 11). The equilibrium with non-vanishing currents (right figure), reproduces the observed indentation on the inboard plasma edge much better, than the nearly currentless equilibrium (left figure).

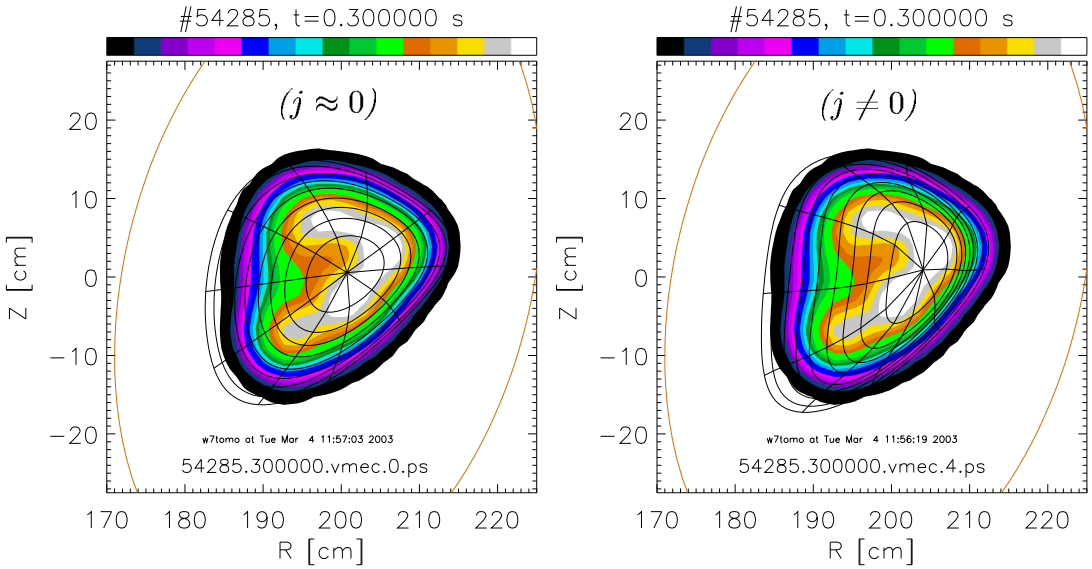


*Fig. 11: Comparision of the calculated equilibria with the tomographic reconstruction.*

## 8 Conclusions

For the determination of the toroidal current density- and iota-profile from soft X-ray measurements, the W7-AS "high-$T_i$" shot #54285 was used, because of the best known pressure profile in this case. After the fitting of the radial emissivity function on the nearly currentless equilibrium, it was possible to optimize this equilibrium by changing the toroidal current density profile. The current density profile, determined so far, consists of a large central counter current density (OH-driven) and a corresponding off-axis co current density (NBI+bootstrap-driven).

The sensitivity of this diagnostic methode depends clearly on the quality of the input data. So, the main conclusion is: With good enough (precise calibrated and a lot of) X-ray measurements, a good enough measurement of the total pressure profile and a good and fast enough equilibrium code, it is practically possible, to determine the toroidal current density- and iota-profile in a stellarator (or tokamak).

Anyway, besides other equilibrium relevant data (like magnetics, MSE, etc.), the SXR measurements can make some contribution to the reconstruction of the plasma equilibrium, and should be included in an integrated equilibrium fit.

## References

[1] Görner C., Ph.D.-Thesis, IPP-III/230 (1998)
[2] Görner C. et. al, Stellarator News, **55** (1998) 2-5
[3] Görner C. et. al, 24th EPS Conf., Berchtesgaden ECA Vol **21A-IV**, 1625 (1997)
[4] Weller A., Görner C., Gonda D., Rev. Sci. Instr., **70** (1999) 484
[5] Hirshman, S.P., Whitson, J.C., Phys. Fluids **26**, 3553 (1983) 12
[6] Klose, S. et. al, 29th EPS Conf., Montreux ECA Vol **26B**, P-5.032 (2002)
[7] Marushchenko,N.B. et.al, 29th EPS Conf., Montreux ECA Vol **26B**, D-5.003 (2002)
[8] Fischer R., Dinklage A., Pasch E., Plasma Phys. Control. Fusion **45** (2003) 1095
[9] Geiger J. et. al, 24th EPS Conf. Contr. Fus. Berchtesgaden **21A** IV (1997) 1617